Monte Carlo Study of Gunn Oscillations in Geometrically-Shaped Planar Gunn Diodes Based on Doped GaN: Influence of Geometry, Intervalley Energy and Temperature

Sergio García-Sánchez, Ignacio Íñiguez-de-la-Torre, Susana Pérez, Tomás González, *Senior Member, IEEE*, and Javier Mateos, *Member, IEEE*

***Abstract*—An investigation into self-switching diodes based on highly doped GaN is conducted under direct current (DC) bias conditions. Different device geometries are explored under various lattice temperatures and polarization scenarios. Also, the impact of adopting an intervalley energy ε_{1-2}=0.9 eV for this material is examined and compared with results obtained with the traditionally accepted value of 2.2 eV. For a rectangular channel configuration, simulations predict oscillation frequencies in excess of 200 GHz, much above the expected transit-time value, due to the fact that the Gunn domains are formed near the anode side of the channel. Conversely, structures with a V-shape geometry are able to start the formation of the Gunn domain inside the channel, thus generating oscillations at much lower frequencies (tens of GHz). The key result is that the lower ε_{1-2} leads to smaller threshold voltage values (and also slightly smaller oscillation frequencies), particularly in diodes with short channels.**

***Index Terms*—Doped gallium nitride (GaN), Gunn diode, Monte Carlo simulations, electronic devices**

I. Introduction

The field of terahertz (THz) science and technology has garnered in recent years significant international attention, despite the challenges it faces. This is mainly due to its promising applications, which cover a wide spectrum of areas. In particular, THz applications range from ultra-broadband wireless transmission to medical diagnostic systems, industrial quality control, security scanners to detect weapons and explosives, THz astronomy, pharmacology, bioscience and biotechnology [1], [2], [3], [4], [5], [6]. Extensive efforts have been dedicated to the advancement of terahertz sources in both the optical and electronic sides. Within different devices architectures explored, Gunn diodes, which exploit the negative differential mobility (NDM) of III-V materials, stand out as a particularly appealing option. Specifically, it is expected (as shown in many theoretical works [7], [8], [9], [10], [11], [12]) that GaN is able to generate high-power high frequency Gunn oscillations because of its larger bandgap and higher electron velocity than other semiconductors like GaAs or InP [13]. However, experimental measurements of vertical GaN Gunn diodes have thus far yielded only indirect evidence of current oscillations [14], [15]. Also, other approach has been explored by considering geometrically-shaped planar Gunn diodes (GS-PGDs) and geometrically-V-shaped planar Gunn diodes (GVS-PGDs), inspired on the self-switching diode concept, which avoids the appearance of large electric fields near the contact terminals [16], [17].

The shape of GVS-PGDs increases the electric fields near the contact terminals and can fix the electrical field at the cathode side of the channel, so that the threshold voltage needed for the onset of the oscillations is reduced. Diodes based on AlGaN/GaN heterojunctions have been explored, expecting to reach high output power at frequencies of hundreds of GHz [17]. Nevertheless, despite simulations predicting the occurrence of Gunn oscillations in GaN diodes [17], [18], no experimental evidence of these oscillations was detected in the fabricated devices. On the other hand, diodes based on a doped GaN active layer have been recently explored instead of the typical AlGaN/GaN epilayers [19]. Monte Carlo (MC) simulations indicate that utilizing highly doped GaN as the active layer can lead to a more efficient generation of Gunn oscillations [20]. However, fabricated shaped nanochannels based on doped GaN active layers show a premature breakdown at low voltages, not linked to thermal dissipation but to an avalanche process [21]. Our suspicion is that the breakdown voltage of the fabricated diodes coincides with the threshold voltage obtained from simulations for the onset of Gunn oscillations, V_{th}, since they can trigger the avalanche process [21]. We have found a good correlation between the experimental breakdown voltage and V_{th} by using a lower conduction band intervalley energy, ε_{1-2}, than that considered for GaN in our previous simulations [19], 2.2 eV, as taken from density functional theory (DFT) calculations [22]. Indeed, recent experiments confirm that ε_{1-2} for GaN could be lower (ε_{1-2}=0.9 eV) [23], [24], [25] than that typically

This work has been partially supported through grants PID2020-115842RB-I00 and PDC2023-145896-I00 funded by MCIN/AEI/10.13039/501100011033, the Junta de Castilla y León and FEDER through project SA136P23 and the Fundación General de la Universidad de Salamanca through project PC_TCUE23-24_011. This research has made use of the high performance computing resources of the Castilla y León Supercomputing Center (SCAYLE, www.scayle.es), financed by the European Regional Development Fund (ERDF). (*Corresponding author: Sergio García-Sánchez*)

S. García-Sánchez, I. Íñiguez-de-la-Torre, S. Pérez, T. González and J. Mateos are with with the Applied Physics Department, and USAL-NANOLAB, Universidad de Salamanca, 37008 Salamanca, Spain (e-mail: sergio_gs@usal.es, indy@usal.es, susana@usal.es, tomasg@usal.es and javierm@usal.es).

considered for this material [22], [26], so that the values obtained for V_{th} are lower, and similar to those for which device breakdown is observed [21], [19]. Surprisingly, most of the simulations of GaN (with the exception of the model used by Sadi $et\,al.$ [27] for the MC simulation of LEDs) and all previous analysis of Gunn oscillations made for GaN devices were performed by using values near to that extracted from theoretical DFT calculations ε_{1-2}=2.2 eV (or other theoretical works providing similar values [28], [29]), instead of the value obtained from experiments, even if already Fang $et\,al.$ [30] noted the controversy between theory and measurements, but chose to discard the experimental values.

The aim of this work is to conduct a study to investigate the behavior of Gunn oscillations in GS-PGDs and its microscopic characteristics through MC simulations by using ε_{1-2}=0.9 eV updating the results previously obtained with ε_{1-2}=2.2 eV in Ref. [19] for homogeneous structures, and analyzing the effect of the channel geometry by considering both rectangular (GS-PGD) and V-shaped channels (GVS-PGDs).

The paper is organized as follows. The MC simulator and the device details are described in Sec. II. Results and discussion are reported in Sec. III. by analyzing the microscopic characteristics of the material and the influence of geometry, temperature and intervalley energy in rectangular GS-PGDs. Also, the behaviour of Gunn oscillations in GVS-PGDs is studied. Finally, the main conclusions are provided.

II. Monte Carlo Simulator and Device Details

For the study of the microscopic characteristics of bulk GaN, a single particle MC tool has been employed, where various scattering mechanisms are included (intervalley, acoustic and optical phonons -both polar and non-polar-, and piezoelectric effects). The conduction band is represented by a three-non-parabolic, spherical valley model, corresponding to the Γ_1, U and Γ_3 points, as typically considered for the Wurtzite structure of GaN studied here [22], [26]. Refs. [26] and [31] provide the details of the parameters taken into account to define the properties of the GaN material. On the other hand, for the analysis of the diodes, calculations are conducted employing an ensemble MC simulator coupled with a two-dimensional Poisson solver [18], [19]. The impact of the surface charge at the semiconductor-dielectric interfaces is integrated through the application of the self-consistent surface-charge model described in Ref. [32]. Within this model, the surface charge at the semiconductor boundaries it is adjusted self-consistently with carrier concentration in the neighbouring zone, leading to a depletion region. Its key influence on nanochannels due to its large surface-to-volume ratio was studied in detail in Ref. [17].

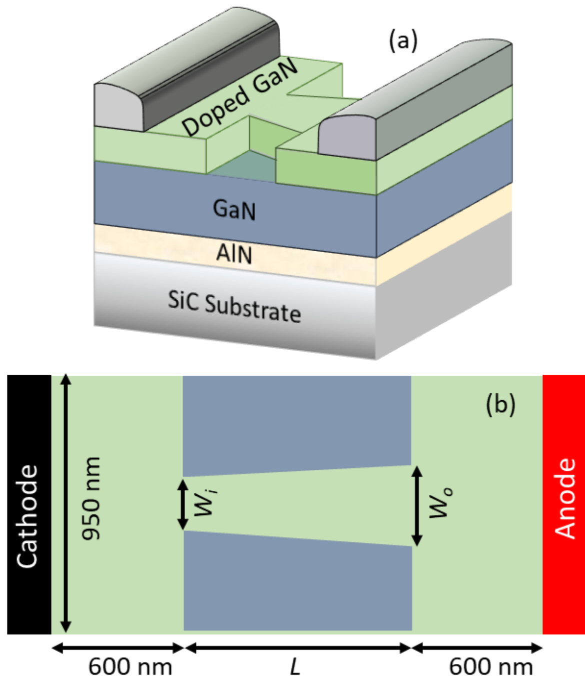

Fig. 1. (a) Three dimensional scheme of an GVS-PGD. (b) Details of the two dimensional geometry of the simulated device.

We have to note that a huge computational effort has been needed for obtaining the results shown in this work, since the total simulated time is 100 ps for each bias point, corresponding to 500.000 steps of 0.2 fs, with more than 2 million electrons included, and a meshing of up to 800x238 cells for the L=2 μ m diodes, so that every single simulation takes more than 2 weeks of computation time.

In Fig. 1(a) and Fig. 1(b), the three-dimensional scheme of an GVS-PGD and the simulated 2D structure are shown, respectively. It is a planar diode in which etching is performed on GaN to define insulating trenches. Diodes with channel lengths L=0.5, 0.75, 1.0, 1.5 and 2.0 μm and different geometries (defined by the channel widths at the input, W_i and output, W_o) have been studied for dopings in the range of 5×10^{17}-10^{19} cm^{-3}. The dielectric permittivity in the trenches region is set to ε_r=1 (air). Simulations are carried out at temperatures of 300 K and 500 K in order to account for the probable self heating effects arising under high-voltage conditions.

III. Results and Discussion

In Fig. 2(a) we present the velocity of electrons obtained through a single particle MC tool for GaN material doped at N_D=5×10^{18} cm^{-3} at room temperature. Up to $\sim$170 kV/cm the value of ε_{1-2} does not have any effect on velocity because electrons do not have enough energy to pass from Γ_1 to U valley, thus remaining in the lower valley. In the inset of 2(a) the electric field for which the velocity reaches its maximum value, E_{peak}, versus N_D is shown. Up to N_D=10^{18} cm^{-3} the peak velocity takes place at an electric field 30 kV/cm lower for ε_{1-2}=0.9 eV, above that doping level this gap is slightly reduced. The valley occupation plotted in Fig. 2(b) shows that the onset of electron transfer from Γ_1 to U valley takes place at electric fields slightly below E_{peak}. Finally, regarding the electron velocity, it is also significantly affected by the choice of the value of ε_{1-2}. The peak velocity decreases from about 2.55 to 2.35×10^7 cm/s when passing from 2.2 to 0.9 eV, while the velocity at intermediate electric fields increases and that at high fields, above 1 MV/cm, remains nearly unchanged (with

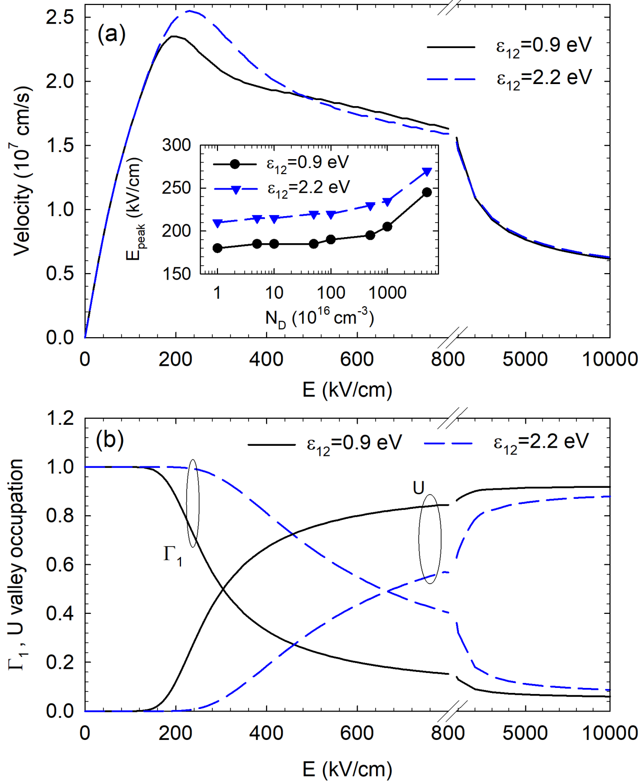

Fig. 2. (a) Average velocity of electrons and (b) valley occupation as a function of the electric field, E, for GaN doped at N_D=5×10^{18} cm^{-3} at room temperature for ε_{1-2}=0.9 and 2.2 eV. The inset shows the electric field at which the velocity reaches its maximum value vs. N_D.

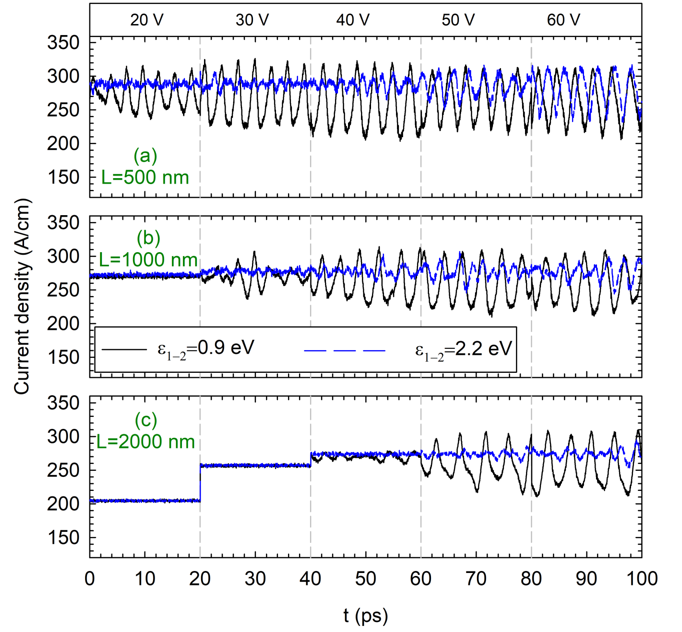

Fig. 3. Time-sequences of the current for GS-PGDs with an active layer doped at N_D=5×10^{18} cm^{-3} and consisting of a single rectangular channel 200 nm wide of length (a) L=0.5 μm, (b) 1.0 μm and (c) 2.0 μm when biases of 20, 30, 40, 50 and 60 V are applied. ε_{1-2}=0.9 and premature eV have been considered and simulations are performed at T=300 K.

a just a slight increase when decreasing ε_{1-2}). Note that such high fields, above the critical field for GaN, may be locally and transiently achieved when a Gunn domain is formed, as we will show later.

Figs. 3(a), (b) and (c) show the time-sequences of the current obtained with MC simulations of GS-PGDs with L=0.5, 1.0 and 2.0 μm, considering for the doped GaN active layer a doping level of N_D=5×10^{18} cm^{-3}. Simulations considering a rectangular channel with a constant width of 200 nm have been done for simplicity, even if tapered channels with V-shape provide the optimum results as reported in Ref. [17]. The first remarkable result is that the oscillation frequencies are above 300 GHz for L=0.5 μm, slightly decreasing when increasing L to around 200 GHz for L=2.0 μm. Surprisingly, these values do not scale with L, and, mainly for the longest devices, are much higher than those expected taking into account the theoretical transit times of the Gunn domains (t_t=L/v_{sat}), which is approximately 75 GHz for L=2.0 μm [obtained taking a value for the saturation velocity v_{sat}=1.5×10^7 cm/s, that corresponding to $E\approx$1 MV/cm in Fig. 2(a)]. Fig. 3 also shows how the intervalley energy ε_{1-2} has a strong influence on the behavior of Gunn oscillations. For example, for the GS-PGD with L=1.0 μm, Gunn oscillations appear at anode-cathode voltages as low as 30 V when considering ε_{1-2}=0.9 eV, but V_{th} increases to around 40 V if the value of 2.2 eV is taken. As the length of the active region increases, V_{th} also increases, scaling approximately with L, as expected. This trend can be better observed in Figures 4 and 5 where we plot the maps of the normalized amplitude of the Gunn oscillations represented by the modulation index, MI. It is defined as MI=I_{pp}/I_m, being I_{pp} the peak-to-peak amplitude of the current oscillations, and I_m the average current.

First, in Fig. 4, where MI is represented $vs.$ L and V for a diode with N_D=5×10^{18}cm^{-3}, we can observe how V_{th} increases almost linearly with length, providing values for the critical electric field, E_{peak}, of around 190 kV/cm for ε_{1-2}=0.9 eV, and slightly higher, 220 kV/cm, for ε_{1-2}=2.2 eV, at T=300 K (increasing to about 220 and 260 kV/cm, respectively, at T=500 K). Such values are quite consistent with those at which the velocity-field curves display NDM in each case. Apart from a higher V_{th}, the amplitude of the oscillations is much higher when decreasing ε_{1-2} from 2.2 to 0.9 eV and when increasing T from 300 to 500 K (even if the effect of T is much lower when using ε_{1-2}=2.2 eV). In Fig. 5 we show the influence of the doping on MI for the diode with L=2.0 μm. Regardless of the value of ε_{1-2}, Gunn oscillations only appear for high doping values starting at around N_D=5×10^{18} cm^{-3}. Also, the influence of ε_{1-2} on the amplitude of the oscillations increases with the doping.

Regarding the frequency of Gunn oscillations, they are estimated to be around 200-300 GHz, highlighting that the Gunn domain is not being formed inside the channel, but near its right end (close to the anode). With the aim of making a more exhaustive study of the formation of the Gunn domains, Fig. 6 shows equidistant instantaneous profiles of the modulus of the electric field for GS-PGDs with L=2 μm and widths W_i=W_o=300 and 400 nm. For the widest channel, simulations are also carried out in the absence of surface charge at the side-

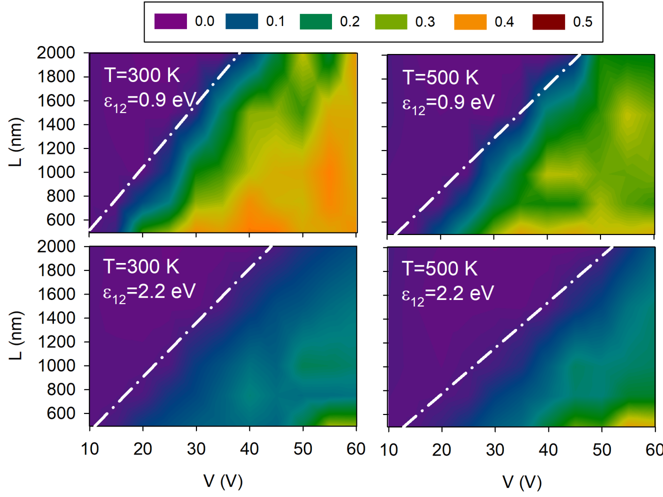

Fig. 4. Maps of MI represented as a function of the applied anode-to-cathode voltage, V, and the length of the active region, L, for N_D=5×10^{18} cm^{-3} for ε_{1-2}=0.9 and 2.2 eV and lattice temperatures T=300 K and 500 K. The dashed lines represent the theoretical values of V_{th} calculated as $E_{peak} \times L$.

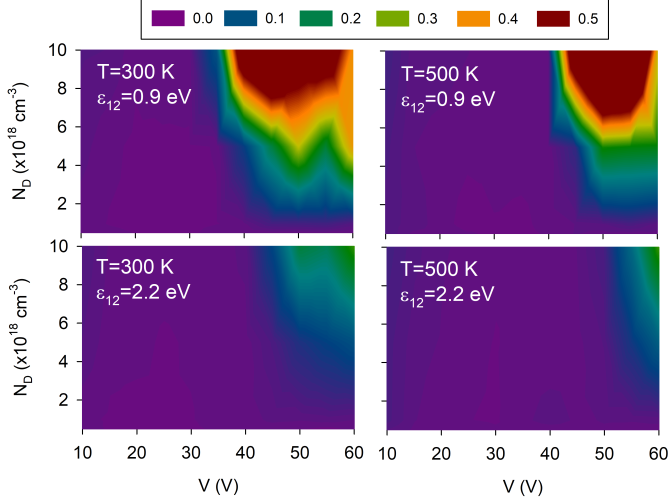

Fig. 5. Maps of MI represented as a function of the applied voltage, V, and N_D for L=2.0 μm for ε_{1-2}=0.9 and 2.2 eV and lattice temperatures T=300 K and 500 K.

walls of the trenches. All cases were simulated for a doping of N_D=5×10^{18} cm^{-3}, a lattice temperature of T=300 K and an applied bias V=50 V. When surface charges are considered, no Gunn oscillations are obtained for ε_{1-2}=2.2 eV, while in the case of 0.9 eV they do appear, with the formation of the high-field domain taking place at the anode side, approximately at the same position regardless of the channel width. However, we cannot say that a Gunn domain is formed in this case, but just space charge waves, in which the carrier motion is not coupled with the shift of the high field zone. This happens because surface charges force the depletion of the channel, more significantly near the anode side, thus enhancing the electric field at that region and avoiding the Gunn domain formation if the electron energy is not enough for transferring to the upper valleys within the channel. Indeed, the surface charge density sharply increases at the anode side of the channel, where high energy electrons are able to reach the semiconductor interface and are trapped at the surface charges, thus strongly reducing the channel width at its exit [17]. In contrast, if surface charges are removed, the diode exhibits Gunn oscillations for both intervalley energies but the formation of the Gunn domain takes place near the center of the channel for the case of ε_{1-2}=0.9 eV, but near the anode end for 2.2 eV (due to a larger "dead space"), thus providing oscillations with much lower frequency in the former case. It is to note that at the bias point represented in Fig. 6(f) Gunn oscillations have a chaotic behaviour, thus leading to the awkward current waveform shown in the inset, with the domain formation happening sometimes near the anode side, but sometimes far from it (this is the case shown in the electric field profiles). That is why the current oscillations are randomly switching from low-amplitude high-frequency oscillations to large amplitude dips with longer periods. It is noteworthy that we have already experimentally observed this chaotic behaviour in InGaAs planar Gunn diodes in conditions where Gunn oscillations are not completely stable [33].

With the aim of favoring the creation of domains within the diode channel, we now study V-shaped diodes (GVS-PGDs). As a first step the current time sequences for increasing V for diodes with L=1.0 and 2.0 μm and widths W_i=100 nm & W_o=200 nm and W_i=200 nm & W_o=300 nm are shown in Fig. 7 (at T=300 K and using N_D=5×10^{18} cm^{-3}). We can observe that V_{th} is lower in comparison with diodes with rectangular channels. Furthermore, the current waveform exhibits a pulse-like nature which corresponds to a clear transit-time dipole-layer mode, in comparison with the sinusoidal-like shape obtained in Fig. 3, which is associated with an accumulation layer mode. Now, lower oscillation frequencies are reached (80-90 GHz for L=1.0 μm and 35-60 GHz for L=2.0 μm) due to the fact that the V-shape channel creates a high electric field at the narrower cathode side of the channel, thus favoring the domain formation close to its entrance.

We plot equidistant (each 2 ps) instantaneous profiles of the electric field for a diode with L=2.0 μm, W_i=100 nm and W_o=200 nm in Fig. 8. The onset of the Gunn domain is estimated to take place at the 0.7-0.8 μm x-position. In this case, since the domain formation starts close to the cathode side of the channel, a rough estimate for the oscillation frequency can be made as f_{osc}=v_{sat}/L_e, where L_e is the effective transit distance calculated as the channel length minus a dead space of about 0.2-0.3μm. This estimation allows to control the oscillation frequency from a manufacturing standpoint, by designing the channel with the desired length and doping level. Note that the domain moves at high velocity during its formation until it is finally mature, then travelling at approximately a constant (saturation) velocity until it reaches the anode. It is remarkable, that the huge electric field reached at the domain position takes values as high as 7 MV/cm, so that the drift velocity of the Gunn domain is much lower than that extraced from the v-E curves of Fig. 2(a) at values below the critical electric field for GaN. We have estimated the values for the Gunn domain drift velocity to be 0.71, and 0.74×10^7 cm/s for ε_{1-2}=0.9 and 2.2 eV, respectively, slightly lower in the former case [and in good agreement with the v-E curves at

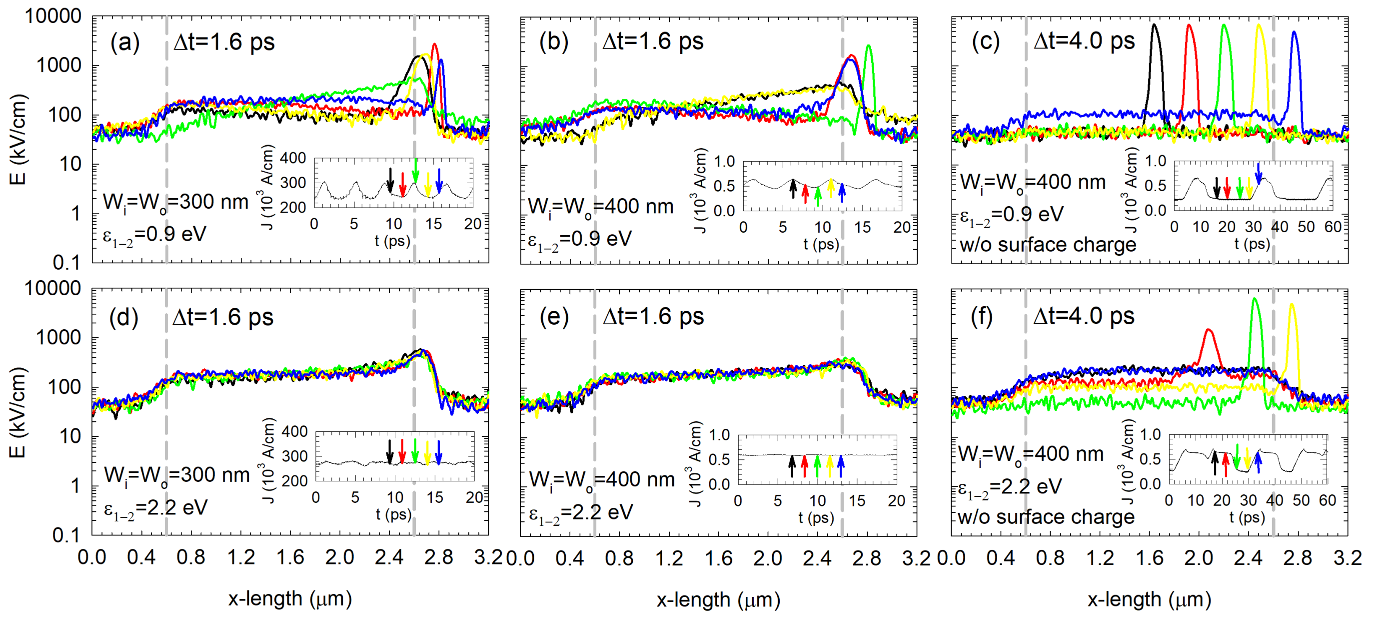

Fig. 6. Instantaneous profiles of the electric field recorded for a 2.0 μm length GS-PGD with N_D=5×10^{18} cm^{-3}, 50 V applied between contacts and a lattice temperature of T=300 K. The two intervalley energies of ε_{1-2}=0.9 and 2.2 eV are considered. Widths of W_i=W_o=300 and 400 nm are analyzed. For the largest width, simulations are also carried out without including the surface charge at the sidewalls of the trenches. The snapshots of the profiles are equidistant with a time shift of 1.6 ps (4 ps in the absence of surface charge). The vertical dashed lines indicate the beginning and the end of the channel. Insets collect the time sequences of current densities, with arrows indicating the time instants where the snapshots of the electric field profiles have been extracted.

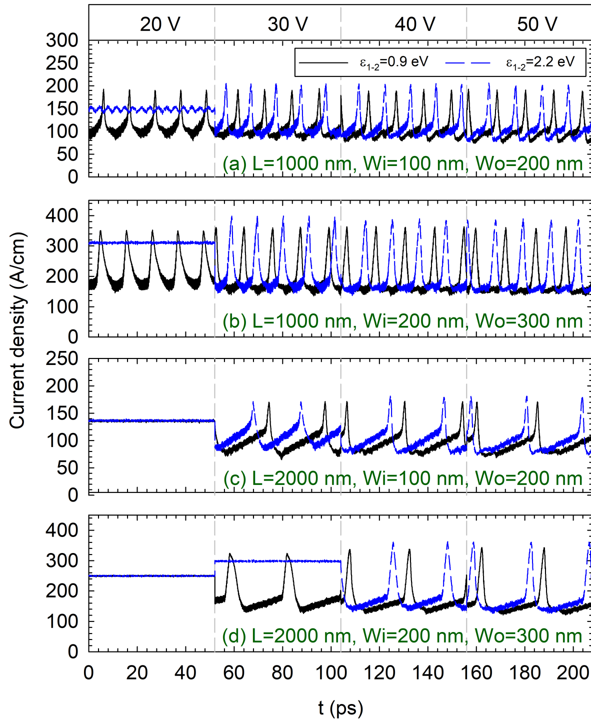

Fig. 7. Current time sequences of GVS- PGDs at 20, 30, 40 and 50 V for lengths of the active region (a) and (b) 1.0 μm and (c) and (d) 2.0 μm and channel widths (a) and (c) W_i=100 nm & W_o=200 nm, and (b) and (d) W_i=200 nm & W_o=300 nm. A doping of 5×10^{18} cm^{-3} is considered at T=300 K.

6-7 MV/cm, see Fig. 2(a)].

The color maps of MI for PGDs with L=2.0 and W_i=200 nm are represented as as function of W_o and V in Figures 9(a) and (b), showing that a lower value of ε_{1-2} favors the generation of Gunn oscillations at lower V, lowering V_{th} for GVS-PGDs with respect to GS-PGDs. It is also interesting that V_{th} decreases when increasing W_o, up to around 280 nm, and then saturates at a value about 30 V for ε_{1-2}=0.9 eV and 35 V for ε_{1-2}=2.2 eV. Moreover, for V>V_{th}, oscillations with a similar amplitude are obtained for both values of ε_{1-2}, but, remarkably, significantly higher values of MI are attained in comparison with the rectangular GS-PGDs (see Fig. 5). Fig. 9(c) shows that the oscillation frequencies (obtained by Fourier transform of the current) of the different considered geometries are in the 35-55 GHz range, decreasing for higher V and being systematically lower for ε_{1-2}=0.9 eV than for 2.2 eV, due to a shorter dead space required for the domain formation (which leads to a longer effective length), as well as the lower electron velocity (as observed in the v-E curves of Fig. 2(a) just above the onset of the NDM). We have to remark that the precision of these values is not very high, with an error of about ±4 GHz due to the small number of simulated periods (3-4 for the lowest oscillation frequencies). Finally, Fig. 9(d) shows how the peak-to-peak amplitude, I_{pp}, of the Gunn oscillations is nearly constant with the variations of ε_{1-2}, but it is sharply reduced when increasing the opening of the channel exit from 275 to 300 nm [exactly the same behavior as that exhibited by MI in Figs. 9(a) and (b), since both quantities are practically proportional]. This happens because such geometry increases the non homogeneity of the electric field, concentrating it at the channel entrance (and thus decreasing the value of V_{th}), but reducing it at the anode side, thus avoiding the maturation of the domain and reducing the amplitude of the oscillations.

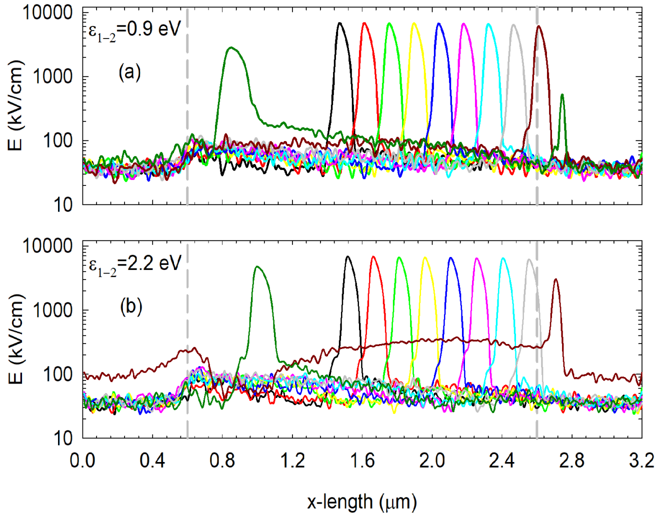

Fig. 8. Instantaneous profiles of the electric field for a bias of V=50 V in a diode with L=2.0 μm, W_i=100 nm and W_o=200 nm. The time shift between the equidistant profiles is 2 ps. The vertical dashed lines indicate the beginning and the end of the channel. (a) ε_{1-2}=0.9 eV and (b) ε_{1-2}=2.2 eV.

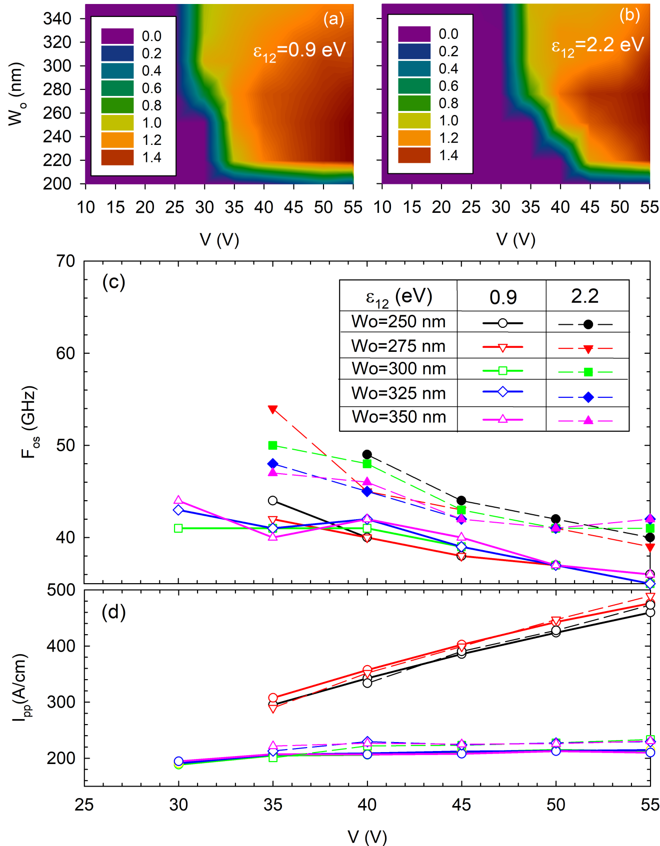

Fig. 9. Maps of MI represented as a function of the applied anode-to-cathode voltage, V, and the exit channel width W_o: (a) ε_{1-2}=0.9 eV and (b) ε_{1-2}=2.2 eV. (c) Oscillation frequency and (d) peak-to-peak current amplitude as a function of V. Diodes with L=2.0 μm, W_i=200 nm and different values of W_o using N_D=5×10^{18} cm^{-3} at T=300 K have been considered.

IV. CONCLUSIONS

GS-PGDs and GVS-PGDs have been studied as candidates for fabricating high power emitters in the THz range. For GS-PGDs, fundamental frequencies of hundreds of GHz are predicted for ε_{1-2}=0.9 eV, with increasing amplitude as the doping of the active layer is increased. In these rectangular geometries, the domain formation is found to take place near the anode end of the channel. For GVS-PGDs, V_{th} is lower thanks to the focusing of the electric field by the smaller width of the channel at its input. This geometrical shaping also leads to the onset of Gunn domains taking place well within the channel, thus originating oscillations of lower frequencies but higher amplitudes, as long as the width of the channel at the exit is not much larger than that at the entrance. The lower value of ε_{1-2} considered in this simulations allows for the onset of oscillations at lower applied voltages both for GS- and GVS-PGDs and with similar amplitudes. Finally, due to the probable self-heating effects arising during the practical operation of the PGDs we have studied the Gunn oscillations at T=500 K and we conclude that they appear at higher voltages with lower amplitudes, but never disappearing.

REFERENCES

[1] P. Sen and J. M. Jornet, “Experimental demonstration of ultra-broadband wireless communications at true terahertz frequencies,” *2019 IEEE 20th International Workshop on Signal Processing Advances in Wireless Communications (SPAWC)*, pp. 1–5, 2019.

[2] T. Amini, F. Jahangiri, Z. Ameri, and M. A. Hemmatian, “A review of feasible applications of THz waves in medical diagnostics and treatments,” *Journal of Lasers in Medical Sciences*, vol. 12, 2021.

[3] D. M. Mittleman, “Twenty years of terahertz imaging,” *Optics express*, vol. 26, no. 8, pp. 9417–9431, 2018.

[4] D. Etayo, J. Iriarte, I. Palacios, I. Maestrojuan, J. Teniente, I. Ederra, and R. Gonzalo, “THz imaging system for industrial quality control,” *2011 IEEE MTT-S International Microwave Workshop Series Millimeter Wave Integration Technologies*, pp. 172–175, 2011.

[5] A. G. Markelz and D. M. Mittleman, “Perspective on terahertz applications in bioscience and biotechnology,” *ACS Photonics*, vol. 9, no. 4, pp. 1117–1126, 2022.

[6] A. Gong, Y. Qiu, X. Chen, Z. Zhao, L. Xia, and Y. Shao, “Biomedical applications of terahertz technology,” *Applied Spectroscopy Reviews*, vol. 55, no. 5, pp. 418–438, 2020.

[7] E. Alekseev and D. Pavlidis, “Large-signal microwave performance of GaN-based NDR diode oscillators,” *Solid-State Electronics*, vol. 44, no. 6, pp. 941–947, 2000.

[8] V. Gruzinskis, P. Shiktorov, E. Starikov, and J. H. Zhao, “Comparative study of 200-300 GHz microwave power generation in GaN TEDs by the Monte Carlo technique,” *Semiconductor Science and Technology*, vol. 16, no. 9, pp. 798—-805, aug 2001.

[9] R. P. Joshi, V. Sridhara, P. Shah, and R. D. del Rosario, “Monte Carlo analysis of ¨GaN-based Gunn oscillators for microwave power generation,” *Journal of Applied Physics*, vol. 93, no. 8, pp. 4836–4842, 04 2003.

[10] E. A. Barry, V. N. Sokolov, K. W. Kim, and R. J. Trew, “Large-signal analysis of terahertz generation in submicrometer GaN diodes,” *IEEE Sensors Journal*, vol. 10, no. 3, pp. 765–771, 2010.

[11] I. P. Storozhenko and Y. V. Arkusha, “Prospects for using gunn diodes based on GaN, AlN AND InN,” *Telecommunications and Radio Engineering*, vol. 71, no. 8, pp. 717–727, 2012.

[12] L. Yang, S. Long, X. Guo, and Y. Hao, “A comparative investigation on sub-micrometer InN and GaN Gunn diodes working at terahertz frequency,” *Journal of Applied Physics*, vol. 111, no. 10, p. 104514, 05 2012.

[13] H. Kroemer, “Theory of the Gunn effect,” *Proceedings of the IEEE*, vol. 52, no. 12, pp. 1736–1736, 1964.

[14] O. Yilmazoglu, K. Mutamba, D. Pavlidis, and T. Karaduman, “First observation of bias oscillations in GaN Gunn diodes on GaN substrate,” *IEEE transactions on electron devices*, vol. 55, no. 6, pp. 1563–1567, 2008.

[15] A. S. Hajo, O. Yilmazoglu, A. Dadgar, F. Küppers, and T. Kusserow, “Reliable GaN-based THz Gunn diodes with side-contact and field-plate technologies,” *IEEE access*, vol. 8, pp. 84 116–84 122, 2020.

[16] A. Song, M. Missous, P. Omling, A. Peaker, L. Samuelson, and W. Seifert, “Unidirectional electron flow in a nanometer-scale semiconductor channel: A self-switching device,” *Applied Physics Letters*, vol. 83, no. 9, pp. 1881–1883, 2003.

[17] J.-F. Millithaler, I. Íñiguez-de-la Torre, A. Iñiguez-de-la Torre, T. González, P. Sangaré, G. Ducournau, C. Gaquière, and J. Mateos, “Optimized V-shape design of GaN nanodiodes for the generation of Gunn oscillations,” *Applied Physics Letters*, vol. 104, no. 7, 2014.

[18] S. García, S. Pérez, I. Íñiguez-De-La-Torre, J. Mateos, and T. González, “Comparative Monte Carlo analysis of InP-and GaN-based Gunn diodes,” *Journal of Applied Physics*, vol. 115, no. 4, 2014.

[19] S. Garcia-Sanchez, I. Íñiguez-de-la Torre, S. Perez, T. Gonzalez, and J. Mateos, “Optimization of the epilayer design for the fabrication of doped GaN planar Gunn diodes,” *IEEE Transactions on Electron Devices*, vol. 69, no. 2, pp. 514–520, 2022.

[20] J. Mateos, T. González, I. Iniguez-De-La-Torre, S. García, S. Pérez, C. Gaquiere, G. Ducournau, M. Lesecq, M. Agrawal, and D. Nethaji, “Design and fabrication of planar Gunn nanodiodes based on doped GaN,” *2019 IEEE Asia-Pacific Microwave Conference (APMC)*, pp. 971–973, 2019.

[21] S. García-Sánchez, M. Abou Daher, M. Lesecq, L. Huo, R. Lingaparthi, D. Nethaji, K. Radhakrishnan, I. Íñiguez-De-La-Torre, B. Vasallo, S. Pérez *et al.*, “On the practical limitations for the generation of Gunn oscillations in highly doped GaN diodes,” *IEEE Transactions on Electron Devices*, vol. 70, pp. 3447–3453, 2023.

[22] F. Bertazzi, M. Goano, X. Zhou, M. Calciati, G. Ghione, M. Matsubara, and E. Bellotti, “Looking for Auger signatures in III-nitride light emitters: A full-band Monte Carlo perspective,” *Applied Physics Letters*, vol. 106, no. 6, p. 061112, 02 2015.

[23] J. Iveland, L. Martinelli, J. Peretti, J. S. Speck, and C. Weisbuch, “Direct measurement of Auger electrons emitted from a semiconductor light-emitting diode under electrical injection: Identification of the dominant mechanism for efficiency droop,” *Phys. Rev. Lett.*, vol. 110, p. 177406, Apr 2013.

[24] M. Piccardo, L. Martinelli, J. Iveland, N. Young, S. P. DenBaars, S. Nakamura, J. S. Speck, C. Weisbuch, and J. Peretti, “Determination of the first satellite valley energy in the conduction band of wurtzite GaN by near-band-gap photoemission spectroscopy,” *Physical Review B*, vol. 89, no. 23, p. 235124, 2014.

[25] S. Wu, P. Geiser, J. Jun, J. Karpinski, D. Wang, and R. Sobolewski, “Time-resolved intervalley transitions in GaN single crystals,” *Journal of applied physics*, vol. 101, no. 4, 2007.

[26] O. Madelung, “Semiconductors: data handbook,” *Springer Science & Business Media, Berlin*, 2004.

[27] T. Sadi, P. Kivisaari, J. Oksanen, and J. Tulkki, “On the correlation of the Auger generated hot electron emission and efficiency droop in III-N light-emitting diodes,” *Applied Physics Letters*, vol. 105, no. 9, p. 091106, 09 2014.

[28] M. Goano, E. Bellotti, E. Ghillino, G. Ghione, and K. F. Brennan, “Band structure nonlocal pseudopotential calculation of the III-nitride wurtzite phase materials system. Part I. Binary compounds GaN, AlN, and InN,” *Journal of Applied Physics*, vol. 88, no. 11, pp. 6467–6475, 12 2000.

[29] W. R. L. Lambrecht and B. Segall in, *Properties of group III nitrides / edited by James H. Edgar.*, ser. EMIS datareviews series ; no. 11. London: INSPEC, Institution of Electrical Engineers, 1994.

[30] J. Fang, M. V. Fischetti, R. D. Schrimpf, R. A. Reed, E. Bellotti, and S. T. Pantelides, “Electron transport properties of $\mathrm{Al}_x\mathrm{Ga}_{1-x}\mathrm{N}/\mathrm{GaN}$ transistors based on first-principles calculations and Boltzmann-Equation Monte Carlo simulations,” *Phys. Rev. Appl.*, vol. 11, p. 044045, Apr 2019.

[31] S. García, I. Iniguez-de-la Torre, S. Pérez, J. Mateos, and T. González, “Numerical study of sub-millimeter Gunn oscillations in InP and GaN vertical diodes: Dependence on bias, doping, and length,” *Journal of Applied Physics*, vol. 114, no. 7, 2013.

[32] I. Iñiguez-De-La-Torre, J. Mateos, T. González, D. Pardo, J. Galloo, S. Bollaert, Y. Roelens, and A. Cappy, “Influence of the surface charge on the operation of ballistic T-branch junctions: a self-consistent model for Monte Carlo simulations,” *Semiconductor Science and Technology*, vol. 22, no. 6, pp. 663–670, 2007.

[33] Y. Lechaux, I. Íñiguez-de-la Torre, J. A. Novoa-López, O. García-Pérez, H. Sánchez-Martín, J. F. Millithaler, D. Vaquero, J. A. Delgado-Notario, V. Clericò, T. González, and J. Mateos, “Comprehensive characterization of Gunn oscillations in $\mathrm{In}_{0.53}\mathrm{Ga}_{0.47}\mathrm{As}$ planar diodes,” *Semiconductor Science and Technology*, vol. 35, no. 11, p. 115009, sep 2020.